Isotopic engineering of silicon

by

Jacoby Jackson

B.S., Texas A&M University, 2017

A REPORT

Submitted in partial fulfillment of the requirements for the degree

MASTER OF SCIENCE

Tim Taylor Department of Chemical Engineering
Carl R. Ice College of Engineering

KANSAS STATE UNIVERSITY
Manhattan, Kansas

2019

Approved by:

Major Professor
Dr. James Edgar

Copyright

Abstract

Isotopically engineering silicon to achieve nearly 100 % pure ^{28}Si crystals has been researched for use in metrology, quantum computing, and in silicon-based integrated circuits. Silicon is naturally composed of three isotopes: ^{28}Si, ^{29}Si, and ^{30}Si with a relative abundance of 92.2%, 4.7%, and 3.1%, respectively.

Use of isotope engineering of silicon was explored in the International Avogadro Project to define Avogadro's constant. The silicon employed for this project must be as isotopically and chemically pure as possible to reduce defects in the crystal lattice.

Isotope engineered silicon has also been researched for utilization in quantum computing. A proposal by B.E Kane has phosphorous donor atoms imbedded in silicon. The nuclear spin of the phosphorous atoms are the qubits for this scheme. Phosphorous has a nuclear spin ($I=\pm 1/2$) and ^{28}Si does not. Isotopically engineered silicon is needed for this scheme to reduce the concentration of ^{29}Si, which also has a nuclear spin of $I=\pm 1/2$ and is a major source of decoherence.

The isotope composition of silicon also affects its phonon related properties. Thermal conductivity is of interest due to the increasing importance of heat management in integrated circuits. Isotopically engineered silicon has a thermal conductivity ten times higher than that of silicon of natural composition at 24 K and is 8% higher at room temperature.

Table of Contents

List of Figures vi

List of Tables viii

Introduction 1

Process to Isotopically Enrich Silicon 2

Synthesis and Purification of Initial Volatile Compounds 3

Separation of Silicon Isotopes 4

Synthesis and Deep Purification of Silane 5

Producing Polycrystalline Silicon 5

Growth of Isotopically Enriched Silicon Crystals 7

Czochralski Growth 7

Float-Zone 10

Chemical Purity 12

Isotope Engineering in Quantum Computing 16

Single-Qubit Operation 20

Two-Qubit Operation 22

CNOT Gates 26

Proof of Concept Experiments for Kane Quantum Computer 27

Coherence Times 29

Thermal Conductivity of Isotopic Enriched Silicon 33

Phonon Effects 34

Isotope Scattering 34

Experimental Results 35

Conclusion and Critical Analysis 38

References 41

List of Figures

Figure 1: Polycrystalline ^{28}Si ingot in a deposition apparatus [8] 6

Figure 2: ^{28}Si concentration along the length of a crystal grown using the Czochralski method[2]. 8

Figure 3: Schematic of oxygen-hydrogen burner used to produce isotopically enriched SiO_2: (1) burner, (2) crucible, (3) protective coating, and (4) crucible holder with rotary drive[14] 9

Figure 4: Floating-zone apparatus[15] 12

Figure 5: Plot of carbon concentration in polysilicon vs silane[11] 16

Figure 6:Schematic of silicon-quantum computer proposed by Kane [17] 18

Figure 7: Schematic of positive voltage applied to the A-gate in Kane quantum computer[17] 21

Figure 8: Nuclear resonance frequency required for operation of a qubit with A-gate energized[5] 22

Figure 9: Two-qubit operation using a J-Gate. The positive voltage applied to the J-gate results in overlap of the electron wavefunction for two donor atoms [17] 23

Figure 10: Energy levels of coupled electron spin systems as a function of J[17] 25

Figure 11: Schematic of phosphorous donors in natural silicon. The random distribution of ^{29}Si changes the local magnetic field around the phosphorous donors causing the atoms to differ quantum mechanically [6] 28

Figure 12:Schematic of phosphorus donors in ^{28}Si. The removal of isotopic impurities results in the phosphorous atoms being quantum mechanically identical. This allows for the nuclear spins to be initialized to the same orientation for quantum computing applications. [6]..... 29

Figure 13 :SEM image of single-qubit device developed by *Morello et al.* at UNSW. The red sphere represents a phosphorous donor, and its nuclear spin by the arrow. The entire device is in a strong magnetic field, B_o. [6] 30

Figure 14: Comparison of Rabi oscillations for single phosphorous qubit in ^{nat}Si (top) and isotopically enriched ^{28}Si (bottom). [6] 32

Figure 15: Thermal conductivity of silicon crystals with different isotope concentrations vs. temperature[23] 37

Figure 16: Ratio of thermal conductivity of isotopically enriched ^{28}Si crystals to ^{nat}Si [23] 38

List of Tables

Table 1: Progress of isotopically enriched ^{28}Si crystals [8] 3

Table 2:Isotopic composition of single crystals grown from polycrystalline silicon using Czochralski growth method[14] 10

Table 3: Carbon impurities in silicon tetrafluoride prepared using Na_2SiF_6 pyrolysis and Si fluorination. Concentrations are in mole percent.[11] 13

Table 4: Concentration of carbon impurities in $^{28}SiH_4$ after synthesis from $^{28}SiF_4$ produced from Na_2SiF_6 pyrolysis and Si fluorination. Concentration in mole percentage.[11] 14

Table 5: Silane carbon impurity concentration after fractional distillation.[11] 15

Table 6: Total spin state and wave function for electron-spin interactions.[17] 24

Table 7: Possible CNOT gate operations.[18] 27

Table 8: Comparison of coherence times for natural and isotopically enriched silicon single phosphorous device [3] 32

Table 9: Isotope concentration of silicon crystals.[23] 36

Introduction

Isotopes are variants of an element that differ in atomic mass. The atomic mass is the sum of the number of protons and neutrons in an isotope's nucleus. The number of protons is identified by an element's atomic number, which is constant for all the element's isotopes. Silicon, for example, has an atomic number of 14 and all isotopes of silicon have 14 protons and the atomic mass for its isotopes will be equal to the sum of 14 and the number of neutrons in the isotope. [1]

Silicon is among the most abundant elements on Earth and is used extensively in microelectronic devices. Silicon, in the element's natural form, has three stable isotopes with atomic masses of 28, 29, and 30. The relative abundance of the isotopes is 92.2%, 4.7%, and 3.1%.[2] Many physical properties of silicon crystals are dependent on their isotope composition including thermal conductivity, lattice constant, and electronic band gap. All these physical properties are important to semiconductor device performance.[3]

Quantum computing is an area of research where isotopically enriched silicon has seen increased interest. Quantum computers exploit quantum-mechanical principles, such as entanglement and superposition, to perform computations.[4] Silicon's large natural abundance and its established use in microelectronics makes it an attractive medium for quantum computing. Isotope engineering has been essential for overcoming many of the barriers that natural silicon has in relation to this technology.[5]

This literature review will examine processes for obtaining isotopically enriched silicon, its physical properties, and its subsequent applications. Recent research that involves improving the process will also be covered. Thermal conductivity is a physical property that is of particular interest because it can be increased by isotopically enriching silicon.

Process to Isotopically Enrich Silicon

The first use of isotopically enriched silicon was by the International Avogadro Coordination (IAC) to accurately define the value of Avogadro's constant.[2] Its goal was to produce silicon crystals with a well-defined number of silicon atom per unit volume and use this to establish a highly accurate definition of a kilogram. Silicon was chosen due to its high crystal quality and chemical purity. Isotope enrichment was needed because the bond length between silicon atoms in the crystal depends on the combination of isotopes present. Fluctuations in bond lengths throughout the crystal needed to be removed to obtain a well-defined number of silicon atoms.[6] The IAC currently produces silicon crystals with a mass fraction of $^{28}Si >$ 99.995%.[2] Excess bulk isotopically enriched silicon from the IAC is currently the main source used in scientific research. [7] The data in Table 1 demonstrates the progress that the IAC has made in growing ^{28}Si crystals up to 2007.

Table 1: Progress of isotopically enriched ^{28}Si crystals [8]

Date	02/2000	04/2001	09/2001	11/2001	12/2001	06/2002	05/2007
^{28}Si enrichment	0.99896	0.9987	0.9993	0.9944	0.9944	0.9998	0.9995
Crystal mass (g)	6	13	19	10.5	32	75	4530

The process to produce isotopically enriched crystals of silicon is composed of five steps: (1) synthesis and purification of initial volatile compounds, (2) separation of silicon isotopes (3) synthesized and deep purification of silane, (4) production of polycrystalline silicon, and (5) growing crystals.

Synthesis and Purification of Initial Volatile Compounds

Silicon tetrafluoride is the starting compound for isotopically enriching silicon and can be synthesized by either direct fluorination of elemental silicon or thermal decomposition of sodium hexafluorosilicate.[2] The reactions for silicon fluorination and thermal decomposition of sodium hexafluorosilicate are shown in equation 1 and equation 2, respectively. Thermal decomposition of sodium hexafluorosilicate occurs between 570-600 °C.[9]

$$\mathrm{Si} + 2\mathrm{F}_2 \rightarrow \mathrm{SiF}_4 \quad (1)$$

$$\mathrm{Na}_2\mathrm{SiF}_6 \rightarrow \mathrm{NaF}_2 + \mathrm{SiF}_4 \quad (2)$$

Separation of Silicon Isotopes

Several techniques have been implemented to separate isotopes including a centrifugation, distillation, hydride, laser decomposition, and electromagnetic method. The distillation method is not commercially viable due to the low relative volatility, or separation factor of different silicon isotopes. [2] The greatest single stage separation factor is 1.0018 for this method, which is extremely low. [2] The laser decomposition and electromagnetic method produce very low yields of isotopically enriched silicon. [2]

The centrifugal method is the most efficient method of separating silicon isotopes.[2] SiF_4 flows through a cascade of gas centrifuges to separate SiF_4 based on molecular mass. Molecular mass is the sum of the atomic mass of all atoms present in a molecule. Fluorine has only one naturally occurring isotope, ^{19}F. Thus, SiF_4 molecules are separated based on silicon isotopes, yielding isotopically enriched $^{28}SiF_4$, $^{29}SiF_4$, and $^{30}SiF_4$. The relative change is isotope concentration after a cycle of centrifugation is approximately 0.1 making a cascade of approximately 100 centrifuges necessary to yield sufficiently isotopically enriched $^{28}SiF_4$.[10] Centrifugation separates the lightest isotope from the heavier materials. Thus, only one stage of centrifugation is needed to produce $^{28}SiF_4$, but additional stages are needed to separate $^{29}SiF_4$ and $^{30}SiF_4$. [10]

Synthesis and Deep Purification of Silane

High purity silane is produced from the reaction of silicon tetrafluoride with calcium hydride as shown below in equation 3.[2] Calcium hydride is prepared by reacting distilled metallic calcium with hydrogen. [11] Isotopically enriched $^{28}SiF_4$ flows though mechanically dispersed calcium hydride in a stainless-steel reactor. Process yields for isotopically enriched silane are 92-94%. [12] Silane is then purified through batch fractional distillation. [11]

$$\mathrm{SiF_4 + 2CaH_2 \rightarrow SiH_4 + 2CaF_2} \quad (3)$$

Producing Polycrystalline Silicon

Typically, polycrystalline silicon with the natural isotope distribution is produced by the thermal decomposition of silane on resistively heated silicon rods. However, isotopically pure silicon cannot be used be grown by this method due to isotope mixing dilution concerns. Instead, molybdenum has been adopted as a suitable substitute as a substrate for the thermal decomposition of isotopically enriched silane. It is stable at high temperatures and can be easily separated from the deposited silicon layers.

Polycrystalline silicon ingots are grown in a two-stage process.

In the first stage layers of isotopically enriched silicon are deposited on molybdenum via thermal decomposition. The reaction for this process is:

$$\mathrm{SiH_4 \rightarrow Si + 2H_2} \quad (4)$$

Polycrystals of silicon up to 3 cm in length have been obtained. The polycrystals of silicon are then connected into a band by high-frequency contactless welding.

In the second stage, polycrystalline silicon in the form of cylindrical rods are grown by the thermal decomposition of silane with the band of silicon produced in the first stage as the substrate. Polycrystalline silicon ingots with diameter of 4-6 mm have been grown using this method. [12] An ingot of polycrystalline ^{28}Si grown using this method is shown in ***Figure 1***.

Figure 1: Polycrystalline ^{28}Si ingot in a deposition apparatus [8]

Growth of Isotopically Enriched Silicon Crystals

Czochralski Growth

Single crystals of semiconductors, such as silicon, are commonly grown by the Czochralski method.[13] A disadvantage of this method when used to grow isotopically enriched silicon is the potential for isotopic dilution due to the dissolution of the quartz crucible, which is used to contain the molten silicon.[2] Quartz is only commercially available with the natural mixture of silicon isotopes.

This has limited applications of the Czochralski method for growing of isotopically enriched silicon.[2] Both experimental results and calculations have led to the conclusion that the Czochralski method is unable to produce ^{28}Si cssrystals with a purity higher than 99.9%. For the Czochralski method to become a viable process for producing isotopically enriched silicon crystals dissolution of the quartz glass must be prevented. The ^{28}Si distribution of a crystal grown using the Czochralski method is shown in **Figure 2**.

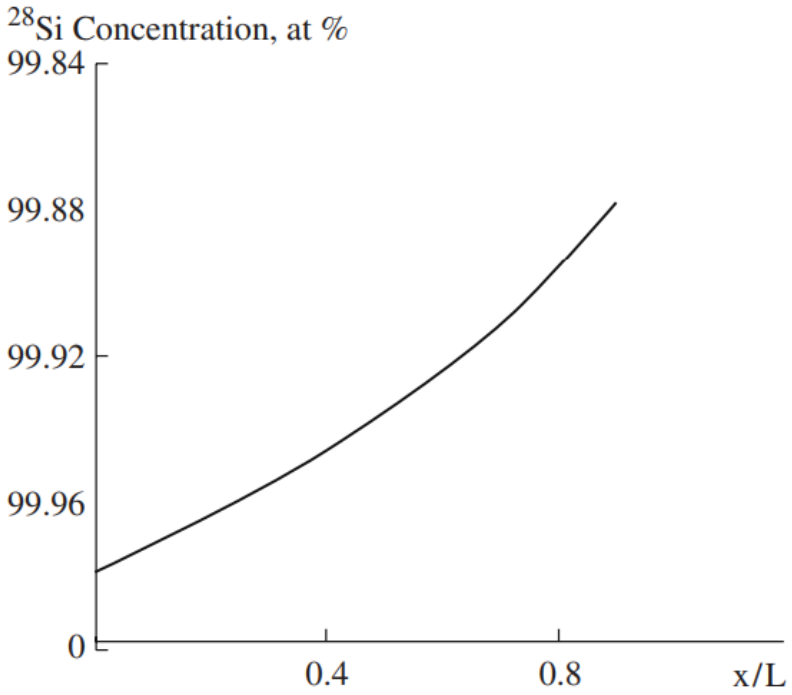

***Figure 2**: ^{28}Si concentration along the length of a crystal grown using the Czochralski method[2]*

To solve this problem, a protective coating of isotopically enriched $^{28}SiO_2$ is deposited on the surface of the quartz crucible.[2] It is produced by oxidizing isotopically enriched silane in the flame of an oxygen-hydrogen burner.[14] This is represented by the following chemical reaction:

$$SiH_4 + 2O_2 \rightarrow SiO_2 + 2H_2O \quad (5)$$

A schematic of a three-channel burner used by *Gusev et al.*[14] is shown in **Figure 3**. High purity hydrogen and enriched silane are introduced through the main channel with oxygen flowing in from the outside chamber. The high temperature of the flame can lead to heating of the burner nozzle and sublimation of the burner material and partial combustion of silane and silicon. To avoid this, argon was introduced to prevent heating of the burner nozzle. The flow

of silicon dioxide produced in the flame was directed towards a pre-heated quartz crucible. *Gusev et al.*[14] recommended a coating thickness of at least 50 µm. Single crystals of isotopically enriched ^{28}Si, ^{29}Si and ^{30}Si were grown using the Czochralski method with a coated crucible. The results are shown in **Table 2**.[14]

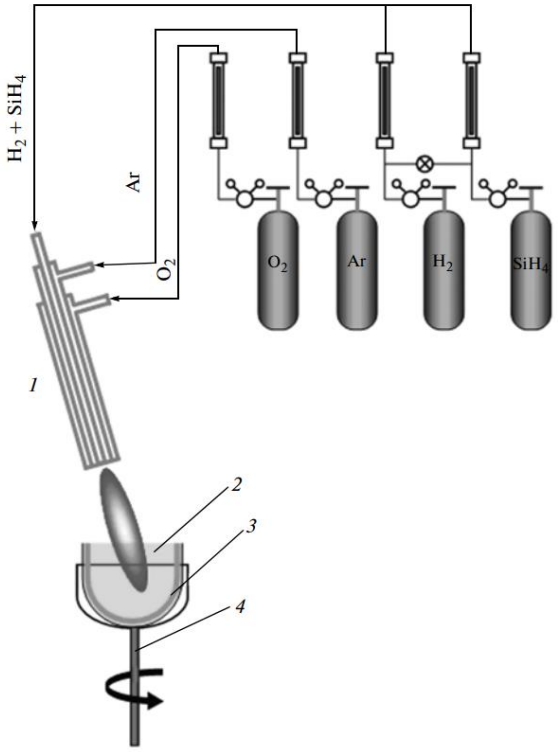

Figure 3: *Schematic of oxygen-hydrogen burner used to produce isotopically enriched SiO_2: (1) burner, (2) crucible, (3) protective coating, and (4) crucible holder with rotary drive*[14]

***Table 2**:Isotopic composition of single crystals grown from polycrystalline silicon using Czochralski growth method[14]*

Main Isotope	Atomic Weight of the Isotope	Polycrystalline Silicon	Single Crystal
28	28	99.9793 ± 0.0046	99.9833 ± 0.0014
	29	0.0170 ± 0.0044	0.0145 ± 0.0012
	30	0.0037 ± 0.0009	0.0022 ± 0.0008
29	28	0.303 ± 0.013	0.563± 0.017
	29	99.487 ± 0.045	99.225± 0.023
	30	0.211± 0.012	0.212± 0.015
30	28	0.0865 ± 0.0094	0.072 ± 0.010
	29	0.1788 ± 0.0517	0.186 ± 0.011
	30	99.7347 ± 0.0525	99.742 ± 0.015

Float-Zone

Float-zone crystal growth (FZ) is currently the most commonly used method to grow single crystals of isotopically enriched silicon from polycrystalline silicon.[2] FZ is a crucible-free process that produces ^{28}Si crystals with higher isotopic and chemical purity than the Czochralski method. No special adjustments are needed, unlike the Czochralski method, to maintain isotope purity.[7] The biggest disadvantage of this method is that the process is much more expensive than the Czochralski method.[13]

The FZ setup consists of polycrystalline silicon rod and a silicon crystal seed that are held on an upper and lower vertical spinning holder, respectively. Between the polycrystalline rod and seed a one-turn RF coil is placed for contactless heating. A schematic of this setup is shown in ***Figure 4***.[15]

The RF coil inductively heats both the polycrystalline feed rod and the seed so that both are partially melted. The seed is then raised to come in contact with the melt. The seed is then pulled downwards, along with a solidifying silicon boule. Chemical impurities generally stay in the molten zone and don't solidify in the boule. [16]

The boule can be further purified by successively passing the RF coil along the boule. Chemical impurities then segregate to the end of the boule. [16]

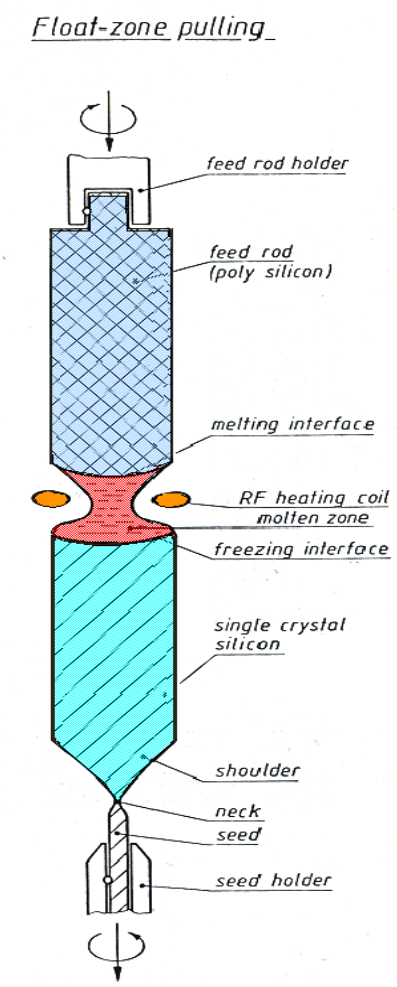

Figure 4: Floating-zone apparatus[15]

Chemical Purity

The polycrystalline silicon obtained from this process is the starting material for growth of single crystals of isotopically enriched silicon. The chemical purity of the polycrystalline silicon influences the purity of single crystals of isotopically enriched silicon. Carbon is one of the most abundant impurities in crystals of isotopically enriched silicon grown using the hydride

method.[2] Carbon impurities affects lattice parameter measurements of isotopically enriched silicon when they are nonuniformly distributed throughout the crystal. ^{28}Si crystals must have minimal impurity concentrations to create a suitable standard for the Avogadro project.

Table 3 shows the concentration of carbon impurities in SiF_4 produced from Na_2SiF_6 pyrolysis and silicon fluorination. Impurity levels were measured using gas chromatography and IR spectroscopy.[11] Silicon fluorination produced significantly less carbon impurities than Na_2SiF_6 pyrolysis. Possible sources for carbon impurities using Na_2SiF_6 pyrolysis include the starting material and the crystal growth apparatus.

Table 3: Carbon impurities in silicon tetrafluoride prepared using Na_2SiF_6 pyrolysis and Si fluorination. Concentrations are in mole percent.[11]

Impurity	Na_2SiF_6 pyrolysis	Si fluorination
CH_4	1.9×10^{-5}	8.5×10^{-6}
C_2H_6	5.6×10^{-4}	1.6×10^{-4}
C_2H_4	3.4×10^{-3}	$< 2 \times 10^{-6}$
C_3H_8	4.4×10^{-5}	$< 2 \times 10^{-6}$
C_3H_6	2.4×10^{-5}	$< 3 \times 10^{-6}$
i-C_4H_8	1.3×10^{-5}	$< 4 \times 10^{-6}$
n-C_4H_8	3.4×10^{-5}	$< 6 \times 10^{-6}$

Table 4 compares the carbon concentration in $^{28}SiH_4$ after synthesis from $^{28}SiF_4$ produced using Na_2SiF_6 pyrolysis and silicon fluorination. Silicon fluorination, once again, was the process yielding lower residual impurity concentrations. The carbon impurity concentrations increased during this step. The total carbon concentration was 102 times higher for the silane produced compared to SiF_4 using silicon fluorination.

Silane is purified by fractional distillation before it is used to synthesis polycrystalline silicon. ***Table 5*** shows the carbon impurities for SiH_4 after fractional distillation. The silane was derived from SiF_4 synthesized by silicon fluorination.

Table 4: Concentration of carbon impurities in $^{28}SiH_4$ after synthesis from $^{28}SiF_4$ produced from Na_2SiF_6 pyrolysis and Si fluorination. Concentration in mole percentage.[11]

Impurity	Na_2SiF_6 pyrolysis	Si fluorination
CH_4	7×10^{-3}	5.0×10^{-3}
C_2H_6	4.0×10^{-4}	3.8×10^{-5}
C_2H_4	1.8×10^{-3}	1.5×10^{-4}
C_3H_8	1.9×10^{-4}	5×10^{-6}
C_3H_6	7×10^{-4}	1.4×10^{-5}
i-C_4H_8	1.6×10^{-4}	4×10^{-6}
n-C_4H_8	8×10^{-5}	4×10^{-6}

Table 5: Silane carbon impurity concentration after fractional distillation.[11]

Impurity	Mole percent
CO	$<3 \times 10^{-5}$
CO_2	$<1 \times 10^{-5}$
CH_4, CHF_3	$<5 \times 10^{-6}$
C_2H_2; C_3H_6; *i*-C_4H_{10}; *n*-C_4H_{10}; C_4H_8 (methylpropene), C_4H_8 (butene -1); C_4H_8 (butene -2); *n*-C_5H_{12}; *n*-C_6H_{14}; *n*-C_7H_{16}	$<2 \times 10^{-6}$
C_2H_4; C_2H_6; C_3H_8; CH_3SiH_3; $C_2H_5SiH_3$	$<1 \times 10^{-6}$
CF_4; *cis*-1,2-$C_2H_2F_2$; $(CH_3)_2SiH_2$	$<4 \times 10^{-7}$
C_2F_4; 1,1-$C_2H_2F_2$; CH_2F_3; $(CH_3)_2CH_2$	$<3 \times 10^{-7}$
CH_2F_3; *trans*-1,2-$C_2H_2F_2$; 1,1,1,2-$C_2H_2F_4$; 1,1,2,2-$C_2H_2F_4$; CH_3Cl; CF_3Cl; $(CH_3)_3SiH$	$<5 \times 10^{-7}$
n-C_9H_{20}	$<4 \times 10^{-6}$
n-C_8H_{18}	$<3 \times 10^{-6}$
C_6H_6	$<2 \times 10^{-7}$
C_6H_5-CH_3	$<2 \times 10^{-7}$
$(C_2H_5)_2SiH_2$	$<6 \times 10^{-7}$

The carbon concentrations in the silane and polycrystalline silicon it produces are strongly correlated. **Figure 5** shows that the carbon concentration in the polysilicon increases with the carbon concentration in the silane, suggesting that silane is the main source of carbon impurities.[11]

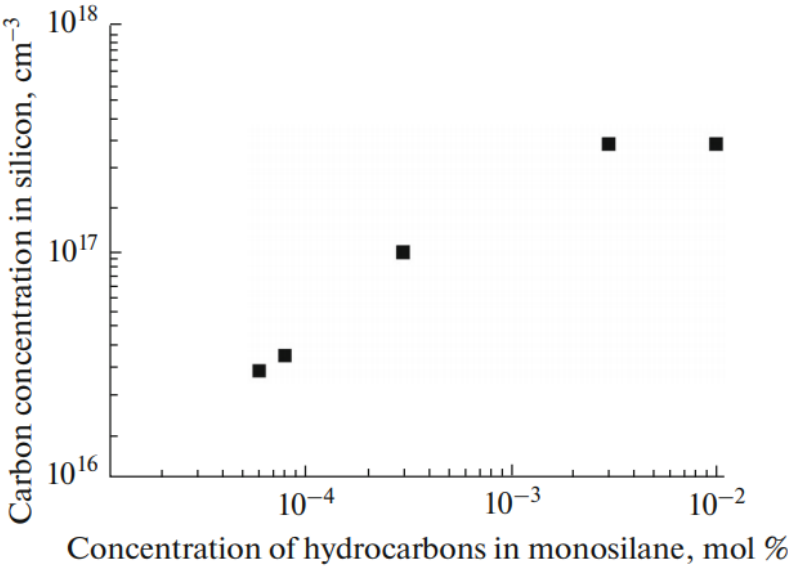

Figure 5:*Plot of carbon concentration in polysilicon vs silane*[11]

Isotope Engineering in Quantum Computing

Quantum computers exploit quantum mechanical-phenomena to manipulate information to perform calculations. Information in quantum computing is represented by qubits (quantum bits), a quantum system that has two distinguishable configurations that correspond to 0 and 1, as in classical computing. The superposition principle applies to qubits and allows its state to be any combination of the two configurations. This greatly enhances the kind of information that can be represented when compared to classical computers.[4]

Isotopically engineered silicon is a good candidate for quantum computing. Silicon is a nearly ideal material due to its large natural abundance and established utilization in microelectronics, such as silicon-integrated circuits. An example of a silicon quantum scheme was proposed by B.E Kane.[5] It implements quantum computation on an array of nuclear spins

located on donors in silicon. Currently this design is scalable to 10 qubits. [4] A schematic of this proposal is shown in **Figure 6**.

Phosphorus-31, the only stable isotope of phosphorous, has a nuclear spin ($I=\pm1/2$). ^{28}Si and ^{30}Si do not have a nuclear spin, but ^{29}Si ($I=\pm1/2$) does. In silicon with a natural distribution of isotopes, the nuclear spin from ^{29}Si can act as source of magnetic noise, disturbing the phosphorous nuclear spin quantum information. This magnetic noise can be eliminated by using isotopically enriched ^{28}Si to eliminate ^{29}Si. ^{28}Si is preferred to ^{30}Si due to its larger relative abundance. Nuclear spins are well isolated from their environment reducing the probability of error for nuclear spin qubits.[6]

Phosphorous acts as *n*-type donor in these devices. Phosphorous, like all common n-type dopants, substitutes on the crystal lattice of silicon. The dopant becomes positively charged by the loss of a valence electron to the lattice structure. At low temperatures, the phosphorous dopant and the free valence electron still interact through Columbic and hyperfine interactions. [13]

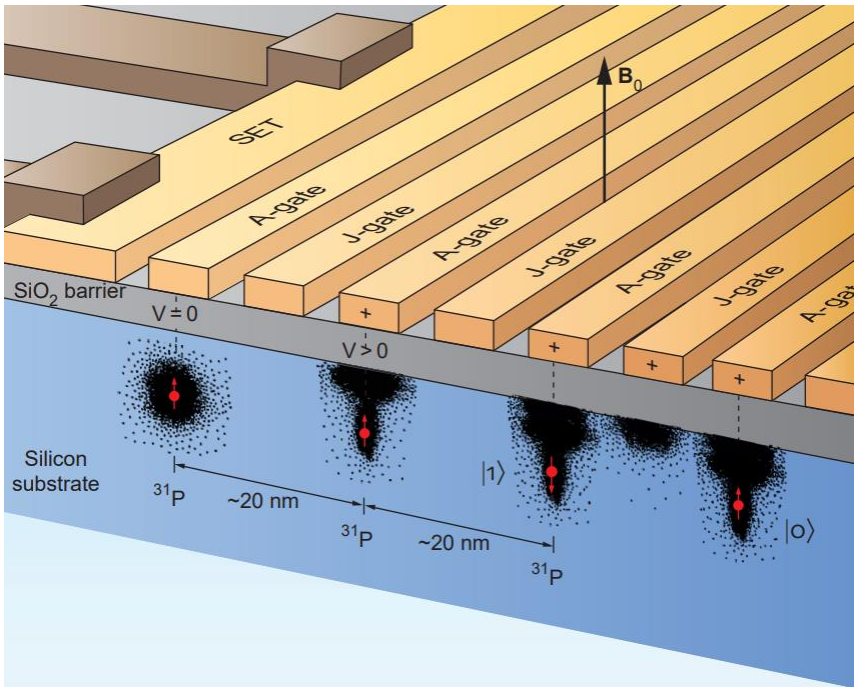

***Figure 6**:Schematic of silicon-quantum computer proposed by Kane* [17]

The interaction of a nucleus and its surrounding is known as the hyperfine interaction.[5] This interaction between the electron spin and phosphorous nuclear spin is exploited in Kane's proposal. The strength of the hyperfine interaction is proportional to the probability density of the electron wavelength function at the nucleus.[5] In silicon, the wavefunction extends over large distances through the crystal lattice. Thus, two nuclear spins can interact with the same electron, leading to electron-meditated or indirect nuclear spin coupling. Since electrons are sensitive to applied electric fields, hyperfine and electron-mediated nuclear spins can be controlled by metallic gates placed on silicon.[5]

The Kane quantum computer uses two types of gates. The A-gate lies directly above the phosphorous donors to individually control single-qubits. J-gates are between qubits and

control electron-mediated coupling between adjacent phosphorous donors, allowing two-qubit interactions.[5] All phosphorus donors must be in a perfectly linear array and are located approximately 20 nm below the gate and are separated from each other by approximately 20 nm.[17] The entire quantum computer must be placed in a strong magnetic field and be at near zero Kelvin temperatures. **Figure 6** displays a schematic of Kane's proposal.

Whether the alignment of the atom's nuclear spin as parallel or antiparallel determines the state of the qubit.[5] The notation for parallel and antiparallel alignments are $|0\rangle$ and $|1\rangle$ respectively. The notation for electron spin is $|\uparrow\rangle$ and $|\downarrow\rangle$.

The magnitude of the hyperfine interaction between spins determines the time required for elementary operations on the qubits and the separation needed between donors in the array. The effective low-energy, low-temperature Hamiltonian describing the interaction between the electron and nuclear spin in a static magnetic field, $\mathbf{B_o}$ is given by equation 6: [5]

$$H = \mu_B \boldsymbol{B}_o \sigma_z^e - g_n \mu_n \boldsymbol{B}_o \sigma_z^n + A\sigma^e \sigma^n \qquad (6)$$

where,

σ^e and σ^n= Pauli spin matrix for electrons, (unitless)

σ^n= Pauli spin matrix for nuclei, (unitless)

μ_B=Bohr magnetron, $\left(\frac{J}{T}\right)$

μ_n=Nuclear magnetron, $\left(\frac{J}{T}\right)$

g_n=Nuclear g-factor, (unitless)

$A\sigma^e\sigma^m$=Hyperfine interaction, (J)

The parameter, A in equation 7 is proportional to magnitude of the electron probability density in the s-orbital, $\psi_e(0)$ and is given by the following equation 7:

$$A = \frac{8}{3}\pi\mu_B\mu_n g_n|\psi_e(0)|^2 \quad (7)$$

At temperates below 10 K, the electron spins are completely spin-polarized in the lower, $|\downarrow\rangle$ state.[17] Thus, only the nuclear spin state of the phosphorous donors is active for single-qubit operation. Assuming the magnetic field, $\mathbf{B}_o$ is aligned on the z-axis, the nuclear spins may be manipulated by applying a second magnetic field, $\mathbf{B}_1$ in the x-direction. The magnetic field, $\mathbf{B}_1$ is given by:

$$\boldsymbol{B}_1 = B_1\cos(\omega_o t)\,\boldsymbol{x} \quad (8)$$

Where ω_0 is the nuclear resonance frequency required for rotation. If this magnetic field is applied, the nuclear spins will begin to rotate and change states.

Single-Qubit Operation

A positive voltage is applied to the A-gate, above each phosphorous donor, to control a single qubit as illustrated in **Figure 7**. The positive charge attracts the electron cloud of the phosphorous atom towards the gate and away from its nucleus. This reduces the magnitude of $\boldsymbol{\psi}_e(0)$, the hyperfine interaction energy, and the resonance frequency required to rotate the nuclear spin. This allows independent single-qubit manipulation. The required nuclear

resonance frequency needed to rotate the nuclear spin at a given applied voltage is shown in **Figure 8**. The orientation of the nuclear spin is fixed when the voltage of the gate is removed.[5,17]

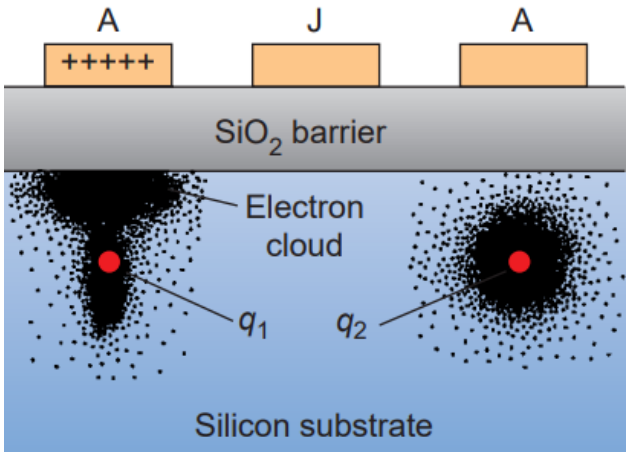

***Figure 7**: Schematic of positive voltage applied to the A-gate in Kane quantum computer*[17]

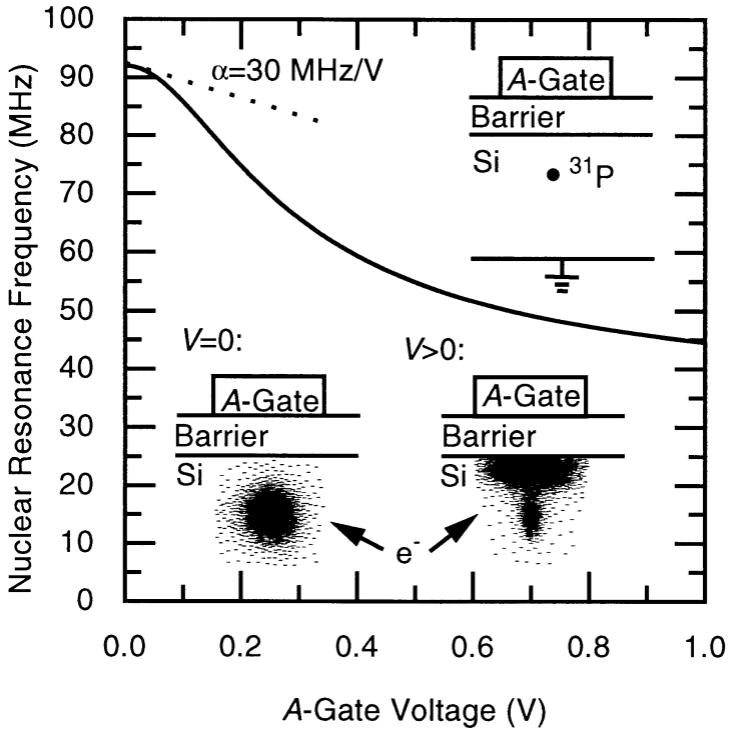

***Figure 8**: Nuclear resonance frequency required for operation of a qubit with A-gate energized*[5]

Two-Qubit Operation

The J-gate controls two-qubit operation. Applying a small positive voltage to the J-gate lowers the potential barrier between the adjacent qubits, causing the electron wave functions of the two donors to overlap, as illustrated in **Figure 9**. The electrons interact with their nucleus at near zero Kelvin temperatures leading to electron-mediated nuclear coupling. [17]

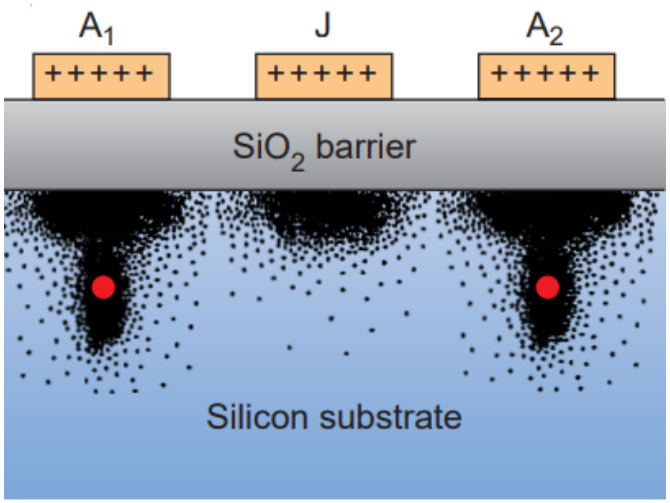

***Figure 9**: Two-qubit operation using a J-Gate. The positive voltage applied to the J-gate results in overlap of the electron wavefunction for two donor atoms* [17]

The effective Hamiltonian for this system describes the complex electron-neutron spin system and is given by the following equation:

$$H_{coupled} = H_1 + H_2 + J\sigma^{1e}\sigma^{2e} \tag{9}$$

The first two terms represent the Hamiltonian for each of the donors and the final term accounts for the spin exchange interaction. J is the exchange coupling coefficient and is proportional to overlap between the electron wave functions. As a result, J is proportional to the voltage applied to the J-gate.[5]

The spin exchange interaction creates 4 coupled electron-spin interaction states, with the total spin, S of which three of these states are equal to 1 and the remaining state equal to 0. The respective wave functions are shown in Table 6.

***Table 6**: Total spin state and wave function for electron-spin interactions.*[17]

Total Spin State, S	Wave Function, $\|S\rangle$
S=1	$\|\uparrow\uparrow\rangle$
	$1\sqrt{2}\,\|\downarrow\uparrow+\uparrow\downarrow\rangle$
	$\|\downarrow\downarrow\rangle$
S=0	$1\sqrt{2}\,\|\uparrow\downarrow-\downarrow\uparrow\rangle$

The energy difference between S=0 and S=1 is equal to the exchange energy, 4J, in the absence of a magnetic field. In the presence of a magnetic field the, $|\uparrow\uparrow\rangle$ and $|\downarrow\downarrow\rangle$, states are separated by $\pm 2\mu_B \mathbf{B}_0$ and the energies of the coupled electron wave functions vary as function of J as seen in **Figure 10**.[17]

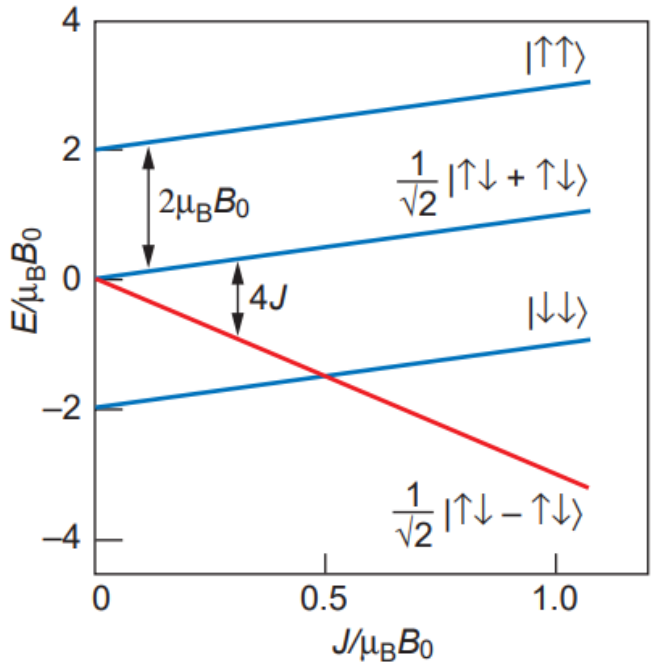

***Figure 10**: Energy levels of coupled electron spin systems as a function of J*[17]

As seen in **Figure 10**, the $|\downarrow\downarrow\rangle$ is the lowest energy step when $J < \frac{1}{2}\mu_o B_o$ and $1/\sqrt{2}|\uparrow\downarrow - \downarrow\uparrow\rangle$ is the lowest energy when $J > \frac{1}{2}\mu_o B_o$. The three blue lines in **Figure 10** have S=1 and the red S=0. In the ground state with $J < \frac{1}{2}\mu_o B_o$ the coupled nuclear-spin states shown as follows in descending order[5] :

$$|11\rangle$$

$$1/\sqrt{2}|\ 10 + 01\rangle$$

$$1/\sqrt{2}\ |\ 10 - 01\rangle$$

$$|00\rangle$$

The shift in energy between the $|11\rangle$ and $1/\sqrt{2}|\ 10+01\rangle$ state and the $|00\rangle$ and $1/\sqrt{2}\ |\ 10+01\rangle$ state are given by[5]:

$$\Delta E = h\omega_A = 2g_n\mu_n B_o + 2A + \frac{2A^2}{\mu_B B_o} \tag{10}$$

The shift in energy between the $1/\sqrt{2}|\ 10+01\rangle\ 1/\sqrt{2}|\ 10-01\rangle$ state is given by[5] :

$$\Delta E = h\omega_J = 2A^2\left(\frac{1}{\mu_B B_o - 2J} - \frac{1}{\mu_B B_o}\right) \tag{11}$$

ω_j is the nuclear exchange frequency and approximates the rate at which binary operations can be performed on the quantum computer.

CNOT Gates

Quantum gates are used to perform a unitary operation on an array of qubits. Implementing quantum gates is essential for successfully operating a quantum computer. Controlled NOT (CNOT) gates are a type of quantum gate that, along with single-qubit operations, form a universal set of gates from which any quantum algorithm can be executed. CNOT gates have two qubits as input with one qubit as the "target" and the other as "control". CNOT gates utilize the quantum-mechanical principal of entanglement to manipulate the nuclear spin of the target qubit if, and only if, the control qubit is in the $|1\rangle$ state. A summary of possible CNOT gate operations is shown in **Table 7**.[18]

Table 7:Possible CNOT gate operations.[18]

Before		After	
Control	Target	Control	Target
$\|0\rangle$	$\|1\rangle$	$\|0\rangle$	$\|1\rangle$
$\|0\rangle$	$\|0\rangle$	$\|0\rangle$	$\|0\rangle$
$\|1\rangle$	$\|0\rangle$	$\|1\rangle$	$\|1\rangle$
$\|1\rangle$	$\|1\rangle$	$\|1\rangle$	$\|0\rangle$

Proof of Concept Experiments for Kane Quantum Computer

Although a qubit must consist of a single quantum, an ensemble of identical qubits can replicate the expected results of a single-qubit. The qubits in the ensemble are initialized to the same quantum state, manipulated together quantum mechanically, and then read out all at once to mimic the performance of a single-qubit. *Itoh et al.*[6] prepared two ensembles following Kane's proposal for quantum computing with one ensemble using natural silicon and the other with isotopically enriched silicon.

In ^{nat}Si the phosphorous donors were quantum mechanically different, but in isotopically enriched ^{28}Si they were identical. The mass difference between the silicon isotopes affected the bond lengths which perturbs the hyperfine interactions between the electron spin and the nuclear spin for each phosphorous donor. This has the potential to shift the NMR frequencies of the phosphorous donors. The random distribution of ^{29}Si also lead to local changes in the

magnetic field near the phosphorous donors, further changing the NMR and electron paramagnetic resonance (EPR). These potential changes to the NMR frequencies of the phosphorous donors emphasize the need for either isotopically enriched ^{28}Si or ^{30}Si for quantum computing.[6] Schematics of the ensembles are shown in **Figure 11** and **Figure 12**.

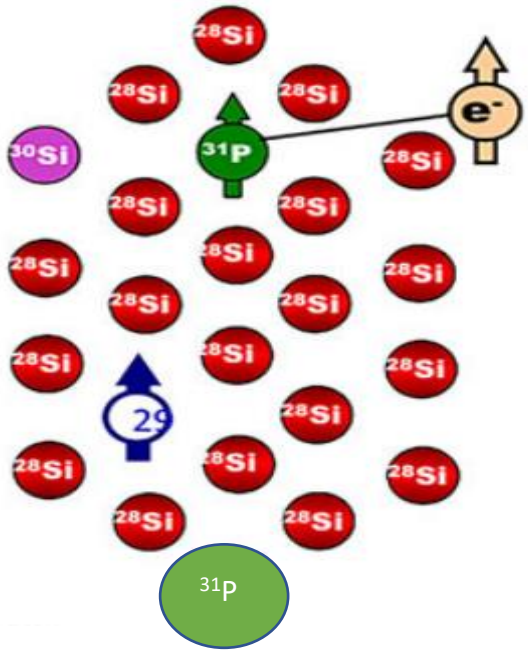

Figure 11: *Schematic of phosphorous donors in natural silicon. The random distribution of ^{29}Si changes the local magnetic field around the phosphorous donors causing the atoms to differ quantum mechanically* [6]

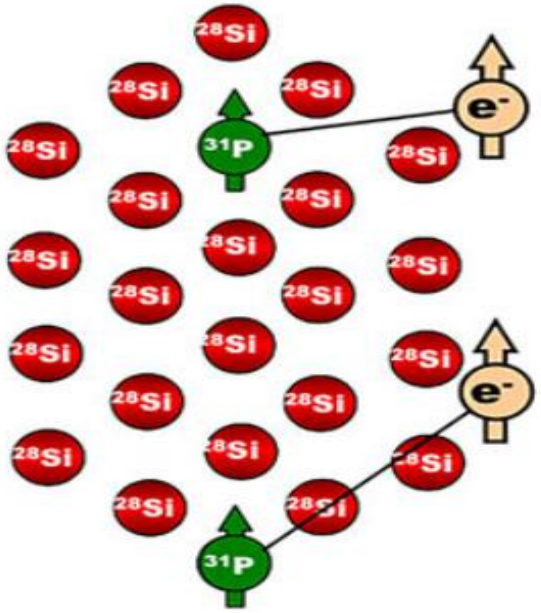

***Figure 12**:Schematic of phosphorus donors in ^{28}Si. The removal of isotopic impurities results in the phosphorous atoms being quantum mechanically identical. This allows for the nuclear spins to be initialized to the same orientation for quantum computing applications.* [6]

Coherence Times

Nuclear spin coherence times (T_2) characterize the time needed for a spin system with a net alignment to reach thermodynamic equilibrium with its surroundings and is an important property for quantum computing. [6] It must be greater than the time needed to complete the quantum computing routine, otherwise the computer will lose information during the calculation.[5] The high crystal quality and low impurity concentrations leaves the ^{29}Si concentration as the likely source of decoherence in natural silicon. Arguably the most important issue associated with demonstrating the viability of silicon-based quantum computing is how far the phosphorous coherence time can be extended by eliminating ^{29}Si. The concentration of ^{29}Si in natural silicon limits the coherence time to approximately 1 ms. [6]

Recent experiments have shown isotopically enriched silicon has a significantly increased coherence time. *Tyryshkin et al.*[19] achieved electron coherence times of approximately 8 s. Research teams at Simon Fraser University were able to obtain coherence times greater than 180 s from the phosphorous donor.[6] These coherence times are both more than enough for quantum computing applications. [6]

These long coherence times were realized in an isolated silicon matrix. For practical quantum computing, devices must be fabricated which requires a variety of foreign materials, including gate insulators and metal contacts. *Morello et al.*[20] at the University of New South Wales (UNSW) developed a single phosphorus qubit device with isotopically enriched silicon which provides a better approximation of the potential of silicon-based quantum computation. The device is capable of initialization, operation, and readout of the quantum information stored in a single electron qubit and the phosphorous nuclear qubit. A scanning electron microscope (SEM) image of the device is displayed in **Figure 13.**

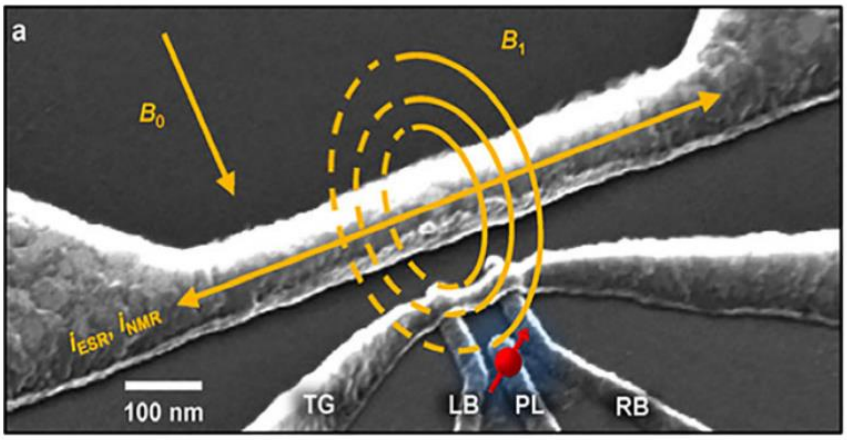

Figure 13 :*SEM image of single-qubit device developed by Morello et al. at UNSW. The red sphere represents a phosphorous donor, and its nuclear spin by the arrow. The entire device is in a strong magnetic field, B_o.* [6]

For comparison, the group also developed an almost identical device with ^{nat}Si. The isotopically enriched device achieved greatly extended coherence times for both the electron and phosphorous donor as summarized in **Table 8**. [6]

Rabi oscillation describes the cyclic behavior of a two-level quantum system, such as qubits, in the presence of an oscillatory driving field.[21] This is studied for quantum applications to describe the probability of a qubit to be in a particular state. The Rabi oscillations for ^{nat}Si and isotopically enriched ^{28}Si differ significantly and re-enforce the need for ^{28}Si in quantum computing. The spin-up probability is the likelihood for a qubit initially in the $|0\rangle$ state to transition to the $|1\rangle$. ^{28}Si predictably cycles between low and high spin-up probability, while ^{nat}Si has ill-defined cycles that don't allow for accurate predictions for the state of a qubit. This phenomenon is demonstrated in **Figure 14**. [6]

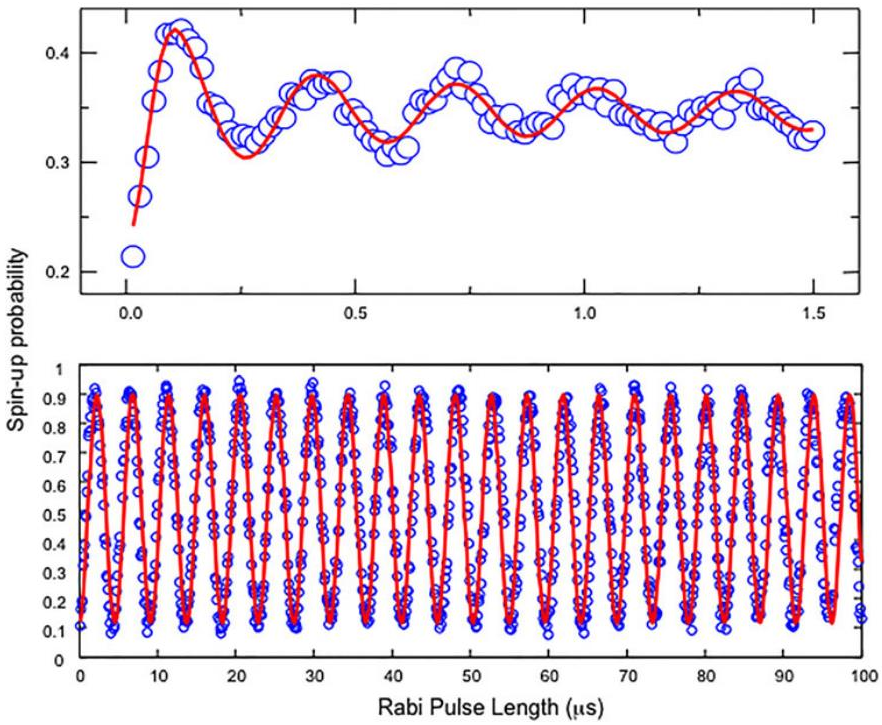

***Figure 14**: Comparison of Rabi oscillations for single phosphorous qubit in ^{nat}Si (top) and isotopically enriched ^{28}Si (bottom).* [6]

***Table 8**: Comparison of coherence times for natural and isotopically enriched silicon single phosphorous device* [3]

	Nat-Si	Si-28
Electron T_2	0.21 ms	0.95 ms
Electrically neutral P donor T_2	3.5 ms	20.4 ms
Electrically positive P donor T_2	60 ms	1.75 s

Thermal Conductivity of Isotopic Enriched Silicon

Integrated circuits (IC) consist of multiple individual components such as, transistors, capacitors, and diodes created from a semiconductor substrate, silicon most commonly, and are connected together to perform a function.[13] As transistor sizes shrink and the number of components continue to rise on silicon-based integrated circuits, the heat produced by these devices increases. The increased power density elevates the device temperatures, which is detrimental to IC performance and reliability. Central processing units (CPUs) are an important and excellent example of a common silicon-based IC. These devices, used in computers and cell phones, have normal operating temperatures ranging from 290-360 K. CPUs operating at temperatures greater than their specified maximum operating temperature can experience reduced performance and elevated risk for damage.[22]

Power management is a critical issue in IC design. Modern ICs have power densities that range up to 40 W/cm^2. The packaging density continues to increase with the operating speed and feature size decreasing for IC, leading to increased heat production in ICs. Elevated temperature reduces the performance and reliability of ICs. Hot spots can also develop in ICs due to non-uniform heat flux further reducing reliability.[22]

The thermal conductivity, symbolized by κ, is a physical property that is affected by isotope concentration.[2] Thermal dissipation in a semiconductor device is limited by the thermal conductivity of the material it is composed of. Thus, the thermal conductivity of a device limits the packing density of transistors that can be implemented without increasing the chances of circuit failure. [22] Increasing the thermal conductivity lowers the peak temperature of a device

for the same power level. Lower temperatures will lead to increased carrier mobility and reduced leakage current. Reducing a device's leakage current will also reduce heat generation. [22]

Phonon Effects

For crystalline solids, such as silicon, the difference in atomic mass between isotopes most directly affects phonon frequencies and phonon related properties, namely the thermal conductivity.[23] Phonons are the elementary vibrational motions of a lattice of atoms oscillating at a single frequency.[1] In chemically pure and defect free crystals the magnitude of the isotope effect is determined by the rate of isotope scattering and phonon-phonon scattering.[23] Eliminating isotope scattering by isotopic disorder in monoisotopic materials, results in a higher thermal conductivity than those composed of multiple isotopes. [2]

Isotope Scattering

Isotope scattering describes phonon scattering due to isotopic disorder caused by the random distribution of isotope in the crystal lattice sites.[23] Isotope scattering sizably increases the thermal resistivity of silicon crystals at room temperature.[23] The non-uniformity of the isotope distribution is quantified by the following formula[24] :

$$g_2 = \sum_i f_i \left(1 - \frac{M_i}{M^2}\right) \quad (12)$$

where,

g_2=isotopic chaos, (unitless)

f_i=molar fraction of component i, (mol of isotope i/total mol)

M_i=Atomic mass of isotope i, (g/mol)

M=Average atomic mass of isotopes in crystal, (g/mol)

Vibrational frequency is inversely related to the mass of the atoms. The simplest dependence of phonon frequency, ω on mass is described by the "spring and ball" model as shown in equation 14:

$$\omega \sim M^{-1/2} \quad (14)$$

The phonon frequencies for the isotopes of silicon all differ, as a result, with ^{28}Si having the highest frequency and ^{30}Si the lowest. In materials with a mixture of isotopes the phonons of different frequency can collide resulting in isotopic scattering.

Experimental Results

The thermal conductivity of silicon with single isotopes and with the natural distribution of isotopes has been measured as a function of temperature, as demonstrated in ***Figure 15***. [23] The isotope composition of the silicon crystals is shown in ***Table 9***. The thermal conductivity of ^{nat}Si is significantly lower than the isotopically enriched ^{28}Si crystals between 10 and 100 K. Small differences in the isotopic purity can greatly affect the thermal conductivity at low

temperatures. The more isotopically pure ^{28}Si crystal A had a significantly higher thermal conductivity than ^{28}Si crystal B between 15 and 32 K. All three crystals experienced maxima in their thermal conductivity at approximately 24 K with ^{28}Si A, ^{28}Si B, and ^{nat}Si having thermal conductivities of about 450, 300, and 40 W/(cm·K) respectively. The thermal conductivity of the two enriched ^{28}Si crystals is roughly equal between 60 and 420 K. This indicates that the thermal conductivity is not a function of isotopic composition for ^{28}Si crystals enriched to 92.92% or greater in this temperature range; phonon-phonon scattering must be considerably larger than isotope scattering in this range.

Table 9: Isotope concentration of silicon crystals.[23]

Crystal	^{28}Si	^{29}Si	^{30}Si
^{28}Si A	99.995	0.0046	0.0004
^{28}Si B	99.92	0.075	0.005
^{nat}Si A	92.223	4.685	3.092

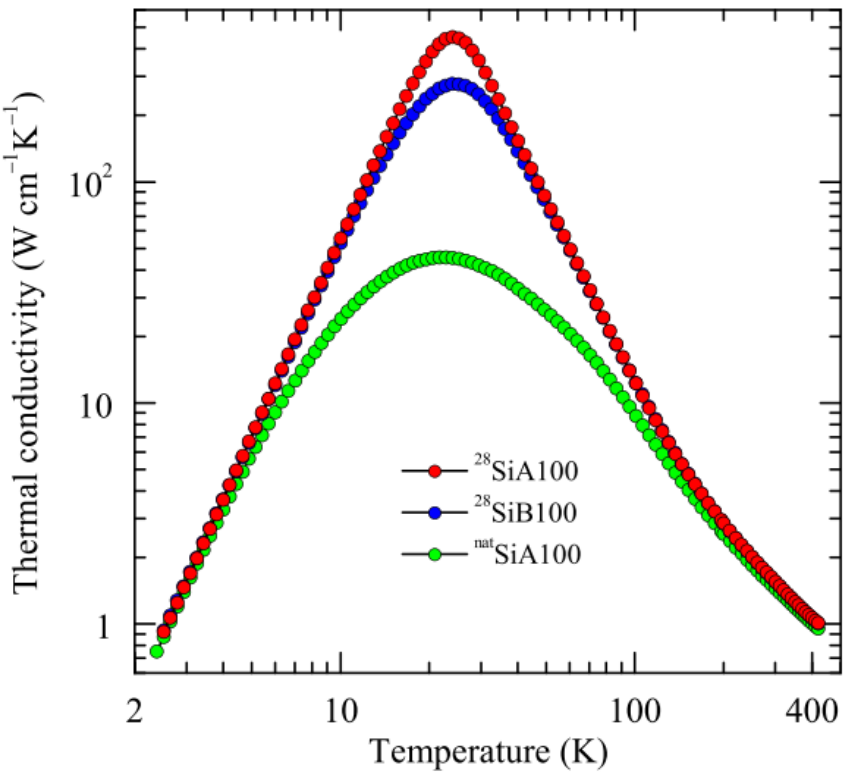

Figure 15: Thermal conductivity of silicon crystals with different isotope concentrations vs. temperature[23]

The ratio of thermal conductivity of isotopically enriched ^{28}Si to ^{nat}Si from 2 to 410 K is shown in ***Figure 16***. The thermal conductivity ratio of the ^{28}Si A crystals reached a maximum of 10 at approximately 24 K. As in ***Figure 15***, the thermal conductivity appears to most strongly depend on isotope concentration in the 10 to 60 K temperature range. At room temperature (298 K) the thermal conductivity was enhanced by a factor of approximately 1.08.

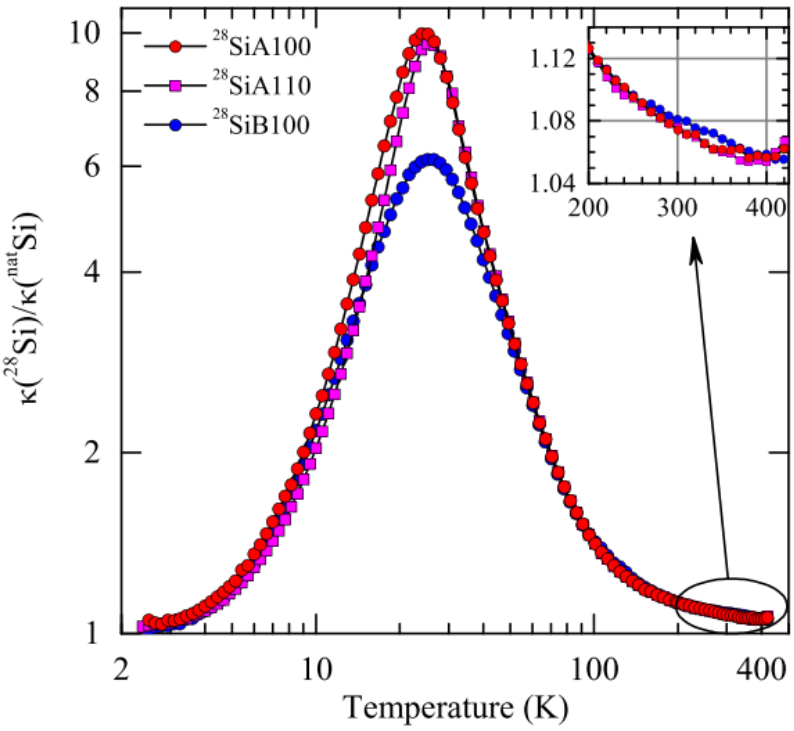

Figure 16: Ratio of thermal conductivity of isotopically enriched ^{28}Si crystals to ^{nat}Si [23]

Conclusion and Critical Analysis

Isotopically enriched silicon has several properties that can make it advantageous when compared to natural silicon. Refining the process to achieve even better isotopic purity silicon will be essential to furthering research and industrial applications of the material. Silicon fluorination should be the preferred method of synthesizing silicon tetrafluoride as it produced materials with a far lower carbon concentration than does Na_2SiF_6 pyrolysis. The strong correlation of silane carbon concentration to polycrystalline carbon concentration is evidence of the importance of using high quality silane for the hydride method.

Due to the high level of isotropic enrichment needed for metrology and quantum computing applications, FZ is best technique for growing isotopically pure crystals. This is

inherently a good technique for growing higher purity single silicon crystals with either the natural distribution or isotopically enriched. Although this technique is more expensive than the Czochralski growth method, the high quality of crystals required justify its use. The protective coating technique discussed in this review does help to relieve concerns regarding concerns regarding isotope dilution, but the use of zone processing for high purity crystals in natural silicon still lead to the conclusion that more research and development will be needed for Czochralski method to be implemented for meteorology and quantum computing applications.

Kane's proposal provides a good framework for silicon-based quantum computers. The proof-of-concept experiments discussed in this review provide evidence of its feasibility. Progress is still needed to realize a functional silicon-quantum computer. The successful demonstration of single-qubit operation is an important milestone to realizing silicon-based quantum computers. The next step needed for this technology is operating quantum gates. The proof-of-concept experiments also provided evidence to the importance of using high purity isotopically enriched silicon. The nuclear spin of ^{29}Si increases the decoherence of phosphorous qubits and disturbs the local magnetic field. This can lead to failure of the quantum computer.

Isotopically enriched ^{28}Si has a higher thermal conductivity than ^{nat}Si due to reduced isotope scattering. This can be beneficial to increase heat dissipation in silicon-based ICs. ^{28}Si crystals enriched to 99.92% have roughly the same thermal conductivity as crystals enriched to 99.995% for common operating temperatures of CPUs (290-360 K). This can be important for the economic feasibility of using isotopically enriched ^{28}Si in CPU chips, as crystals can be grown to the level of enrichment using the Czochralski growth method, which is less expensive than

the float zone melting technique needed to produce crystals for metrology or quantum computing reasons.

References

1. Haller EE. Isotopically engineered semiconductors. *Journal of Applied Physics*. 1995;77(7):2857-2878. https://www.osti.gov/biblio/6457768. doi: 10.1063/1.358700.

2. Gusev A, Bulanov A. High-purity silicon isotopes 28Si, 29Si, and 30Si. *Inorg Mater*. 2008;44(13):1395-1408. doi: 10.1134/S0020168508130013.

3. Itoh KM, Watanabe H. Isotope engineering of silicon and diamond for quantum computing and sensing applications. *MRS Communications*. 2014;4(4):143-157.

4. Knill E. Physics. Quantum computing. *Nautre*. 2010;463.

5. Kane BE. A silicon-based nuclear spin quantum computer. *Nature*. 1998;393(6681):133-137. http://dx.doi.org/10.1038/30156. doi: 10.1038/30156.

6. Itoh KM, Watanabe H. Isotope engineering of silicon and diamond for quantum computing and sensing applications. *MRS Communications*. 2014;4(4):143-157. https://search.proquest.com/docview/1640906273. doi: 10.1557/mrc.2014.32.

7. Dwywer KJ, Pomery JA, Simons DS. Enriching 28Si beyond 99.9998 % for semiconductor quantum computing. *Journal applied physics*. ;47.

8. Abrosimov NV, Aref'ev DG, Becker P, et al. A new generation of 99.999% enriched 28Si single crystals for the determination of avogadro's constant. *Metrologia*. 2017;54(4):599-609. doi: 10.1088/1681-7575/aa7a62.

9. Krylov V, Sorochkina T, Bulanov A, Lashkov A. C1–C4 hydrocarbon release in the preparation of SiF4 through Na2SiF6 pyrolysis. *Inorg Mater*. 2012;48(1):7-9. doi: 10.1134/S0020168511120089.

10. Itoh KM, Kato J, Uemura M. High purity isotopically enriched 29Si and 30Si single crystals: Isotope separation, purification, and growth
. *Japapn Society of Applied Physics*. 2003;42:6248-6251.

11. Bulanov AD, Gavva VA, Sozin AY, et al. Sources of carbon impurities in the preparation of high-purity monoisotopic 28.sup.si by a hydride method. *Inorganic Materials*. 2018;54(10):977. doi: 10.1134/S0020168518100047.

12. Abrosimov NV, Aref'ev DG, Becker P, et al. A new generation of 99.999% enriched 28Si single crystals for the determination of avogadro's constant. *Metrologia*. 2017;54(4):599-609. doi: 10.1088/1681-7575/aa7a62.

13. Ghandhi SK. *VLSI fabrication principles:Silicon and gallium arsenide.* United States of America: Wiley-Interscience.

14. Gusev AV, Gavva VA, Kozyrev EA, Riemann H, Abrosimov NV. Crucibles for czochralski growth of isotopically enriched silicon single crystals. *Inorganic Materials*. 2013;49(12):1167-1169. doi: 10.1134/S0020168513120078.

15. Foll H. Float zone crystal growth. Electronic Materials Web site. https://www.tf.uni-kiel.de/matwis/amat/elmat_en/index.html. Accessed July, 9, 2019.

16. Riemann H, Luedge A. Floating zone crystal growth

. In: *Crystal growth of si for solar cells.* Springer Link; 2009:41-42.

17. Clark R, Hammel C, Dzurak A, et al. Toward a silicon-based

nuclear-spin quantum computer. *Los Alamos Science*. 2002:284-301.

http://dx.doi.org/10.1038/30156.

18. Wilmott CM. On swapping the states of two qubits. *International Journal of Quantum Information*. 2011;9(6):1511-1517.

http://www.worldscientific.com/doi/abs/10.1142/S0219749911008143. doi:

10.1142/S0219749911008143.

19. Alexei M Tyryshkin, Stephen A Lyon, AV Astashkin, AM Raitsimring. Electron spin relaxation times of phosphorus donors in silicon. *Physical Review B*. 2013;68(19):193-207.

20. Andrea Morello, Jarryd J Pla, Floris A Zwanenburg, Kok W Chan, Kuan Y Tan, Hans Huebl, Mikko Möttönen, Christopher D Nugroho, Changyi Yang, Jessica A van Donkelaar, Andrew DC Alves, David N Jamieson, Christopher C Escott, Lloyd CL Hollenberg, Robert G Clark, Andrew S Dzurak. Single-shot readout of an electron spin in silicon. *Nature*. 2010;467(7316):687.

21. Fischer K, Hanschke L, Kremser M. Pulsed rabi oscillations in quantum two-level systems: Beyond the area theorem. *Quantum Science and Technology*. 2017;3.

22. Sheng-Chih Lin, Banerjee K. Cool chips: Opportunities and implications for power and thermal management. *TED*. 2008;55(1):245-255. https://ieeexplore.ieee.org/document/4408792. doi: 10.1109/TED.2007.911763.

23. Inyushkin AV, Taldenkov AN, Ager JW, et al. Ultrahigh thermal conductivity of isotopically enriched silicon. *Journal of Applied Physics*. 2018;123(9):95112. http://dx.doi.org/10.1063/1.5017778. doi: 10.1063/1.5017778.

24. Sellan, DP, Landry, ES, Turney, JE. Condensed physical matter. *Physics rev.* 2010.